Novel underactuated grippers with torque-driven bistable mechanism for alternating grasping and unlimited twisting modes

Mechanism and Machine Theory 228 (2026) 106530

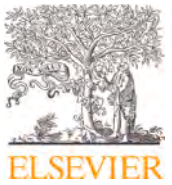

Contents lists available at ScienceDirect

Mechanism and Machine Theory

journal homepage: www.elsevier.com/locate/mechmt

Research paper

Novel underactuated grippers with torque-driven bistable mechanism for alternating grasping and unlimited twisting modes

Andrea Botta *, Luigi Tagliavini, Francesco Amodio, Daniel Pacheco Quinones, Danilo Stimolo, Giuseppe Quaglia, Daniela Maffiodo

Department of Mechanical and Aerospace Engineering (DIMEAS), Politecnico di Torino, Corso Duca degli Abruzzi 24, Torino, 10129, Italy

ARTICLE INFO

Keywords:
Underactuated gripper
Bistable mechanism
Epicycloidal gearing
Ball-spline mechanism
Ball detent torque limiter
Permanent magnet torque limiter

ABSTRACT

This paper presents the design and prototyping of a novel class of underactuated robotic grippers capable of alternating between stable grasping and continuous bidirectional twisting, named Mode-Retentive Underactuated Mechanisms (MRUM). The core of the design integrates a two-degree-of-freedom mechanical transmission with a bistable elastic element, enabling automatic transition between grasping and twisting modes. The bistable element transitions between stable states are triggered through torque limiters, allowing the gripper to autonomously switch states when a torque overload occurs without sensing, control logic, or additional actuators. This dual functionality makes the gripper particularly suitable for manipulation tasks that involve both holding and rotary motion, such as operating manual valves or performing screwing and unscrewing operations. Two prototypes were developed and tested to validate the design principles and demonstrate practical feasibility. The proposed solutions offer a compact approach for complex in-hand manipulation with a single actuator.

1. Introduction

Robotic grippers are among the most widely used end-effectors in robotics, enabling effective manipulation tasks of a diverse range of objects. In the simplest implementation, each degree of freedom (DoF) of the gripper is actuated independently by a dedicated actuator. However, this approach may become an issue when the gripper has multiple DoF, as it increases the complexity of the actuation system and adds weight to the end-effector. Yet, it is not mandatory that all DoF must be actuated. Underactuated systems can be designed in which some DoF are directly controlled by an actuator while others are left passive, allowing them to adapt to the tasks through the dynamics of the system. This design strategy significantly reduces mechanical complexity, weight, and cost, while enhancing robustness and adaptability, especially for unstructured interactions.

In this context, many underactuated grippers have been proposed over the years to reduce the number of actuators and the weight of the gripper required to accomplish the desired tasks. The majority of the proposed solutions exploit passive DoF to allow the gripper to adapt its shape to the object being grasped. Many designs [1–3] implement underactuated finger mechanisms based on the

* Corresponding author.
E-mail addresses: andrea.botta@polito.it (A. Botta), luigi.tagliavini@polito.it (L. Tagliavini), francesco.amodio@polito.it (F. Amodio), daniel.pacheco@polito.it (D. Pacheco Quinones), danilo.stimolo@studenti.polito.it (D. Stimolo), giuseppe.quaglia@polito.it (G. Quaglia), daniela.maffiodo@polito.it (D. Maffiodo).

https://doi.org/10.1016/j.mechmachtheory.2026.106530
Received 22 January 2026; Received in revised form 3 June 2026; Accepted 13 June 2026
Available online 27 June 2026

architecture introduced by Laliberté and Gosselin [4], which consists of linkages and springs. More recently, these finger architectures have evolved by incorporating compliant mechanisms instead of discrete elastic elements [5–7].

There are also more specialised underactuated grippers designed to perform a secondary task after grasping an object, with their design strongly influenced by the intended application. For example, Kakogawa et al. [8] developed a three-fingered underactuated gripper capable of pulling an object closer after grasping it. Using a similar architecture, Ko [9] proposed a tendon-driven parallel gripper that can rotate the grasped object to achieve a more secure hold. Quaglia et al. [10] designed an underactuated gripper capable of cutting fruit stems while maintaining a secure grasp for harvesting tasks.

To the authors' knowledge, with the exception of Nishimura et al. [11,12] and Jang et al. [13], no attempt has been made to develop a robotic gripper with a wrist mechanism that rotates infinitely by using a single actuator. In Nishimura et al. [11,12], an underactuated gripper based on a differential gearing architecture was developed, enabling the gripper to alternate between grasping and twisting motion depending on the dynamic contact conditions. Specifically, the gripper first grasps an object and then rotates in one direction. However, when the actuator reverses direction, the gripper releases the object and begins rotating in reverse only once the gripper is fully open. While this behaviour may be suitable for certain tasks, such as the one proposed in Nishimura et al. [11], the inability to rotate in both directions while keeping an object grasped is quite limiting, in particular for operations such as valve turning or screwing, which require bidirectional rotation while securely grasping an object.

Jang et al. [13] addressed this limitation by introducing a modified grasping mechanism based on a twisted underactuated structure capable of generating finger contraction independently of the input rotation direction. As a result, the gripper closes its fingers regardless of whether the input motion is clockwise or counterclockwise and, once the object is grasped, can rotate in the commanded direction. Nevertheless, when the direction of the input motion is reversed, the elastic restoring behaviour of the mechanism causes the fingers to progressively reopen before re-establishing the grasp in the opposite direction. Consequently, although the mechanism enables bidirectional rotation, it does not maintain a continuous and secure grasp during direction reversals.

This work addresses that limitation by introducing a novel underactuated gripper capable of both firm grasping and continuous bidirectional rotation using a single actuator. A latching mechanism is employed to maintain the system in its current operational mode (grasping or twisting), regardless of the direction of the actuator's motion, achieving a form of mode retention. A purely mechanical torque-driven trigger enables switching between the two modes: a specific torque threshold is defined for each mode, and whenever the actuator exceeds this threshold, the latching mechanism engages and switches the system to the alternate mode of operation. This design allows the gripper to perform common automation tasks such as valve turning, screwing, or any other application that requires both a secure grasp and the ability to rotate an object in both directions using only one motor.

In this work, the general architecture of the Mode-Retentive Underactuated Mechanism architecture is introduced and, based on that, two possible 2-DoF transmission systems and two bistable mechanisms are investigated, even though different combinations of the proposed subsystems or even different ones can be made to design mechanisms falling in the MRUM architecture definition. Section 2.1 presents two transmission systems having two degrees of freedom, namely, an epicyclic gear train and a Ball screw spline - based transmission. Then, Section 2.2 introduces two possible alternatives to achieve a torque-driven bistable mechanism: a ball-detent torque limiter and a permanent magnet torque limiter.

To summarise, while the architectures proposed by Nishimura et al. [11,12] and Jang et al. [13] represent a significant advancement, the proposed MRUM described in this work introduces three fundamental novelties that address the limitations of existing single-actuator systems:

- Bidirectional Operational Stability: Unlike previous designs that release the grasped object upon motor reversal, the proposed system maintains a secure grasp regardless of the actuator's direction.
- Direction-Independent State Retention: The proposed architecture employs a torque-threshold state retention mechanism that ensures the gripper remains in its current operational mode (grasping or twisting) until a specific torque limit is exceeded.
- Novel Mechanical Realisations: We introduce two unique hardware implementations for autonomous mode switching: a ball-detent bistable latch and a magnetic coupling bistable shuttle, both of which eliminate the need for electronic sensors or active control logic. However, different implementations can be designed by combining the presented subsystems differently or using alternative mechanical principles able to achieve the desired behaviours, i.e., underactuated 2-DoF transmissions and torque/force-driven bistable latching elements.

The proposed MRUM should not be interpreted as a single gripper design, but rather as a broader underactuated mechanism architecture combining a 2-DoF transmission, a torque-triggered latching subsystem, and a bistable mode-retention mechanism. Table 1 compares the proposed architecture with representative robotic manipulation systems sharing partial similarities in underactuation, autonomous mechanical switching and mode retention.

Unlike the other systems, MRUM architectures simultaneously combine underactuation, autonomous torque-triggered mode switching, continuous twisting capability, and persistent mode retention within a generalised mechanism architecture.

The functional design of this architecture is detailed in the next section, with particular emphasis on its three main components: the gearing system, the bistable mechanism, and the torque limiter. Two prototypes, primarily fabricated through 3D printing, were developed to validate the design. These same prototypes were used for the experimental validation of the proposed concept through a representative use-case scenario involving opening and then closing a manually operated valve.

Table 1
Comparison of MRUM with state-of-the-art multi-mode underactuated grippers.

Gripper Retention	Actuators	Modes	Auto Switch	Mode
Conventional grippers	2	grasping / twisting	No	No
Nishimura et al. [11]	1	grasping / twisting	Yes	No
Nishimura et al. [12]	1[a]	grasping / twisting	Yes	No
Jang et al. [13]	1[a]	grasping / twisting	Yes	No
Meng et al. [14]	1	grasping / fastening[b]	Yes	No
Seino et al. [15]	0[c]	grasping / twisting	Yes	Yes
MRUM (proposed)	1	grasping / twisting	Yes	Yes

[a] Uses the robot arm's terminal joint.
[b] Grasping and fastening modes are not decoupled. The fastening mode is always active.
[c] Operates by being pushed against the object.

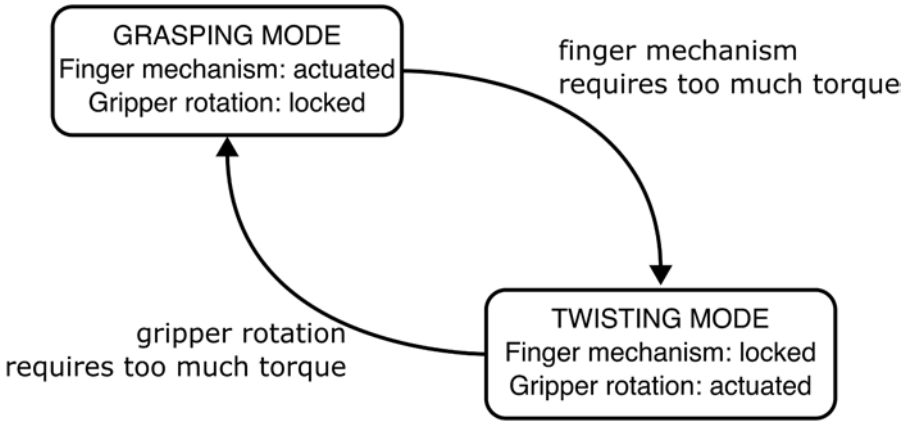

Fig. 1. Simplified state machine of the working principle of the proposed MRUM architecture when used as a gripper.

2. Functional design

The objective of this work is to propose the general architecture of a MRUM to drive the design of different underactuated grippers that can perform grasping and twisting tasks using a single actuator. A dedicated latching mechanism is used to select and retain which mode of operation is employed purely based on the reaction torque applied to the gripper. In other words, the mechanical transmission transmits power to only one mode of operation, realising the corresponding movement while the other one is locked by the latch. As soon as the torque required to actuate the current mode of operation is larger than a set threshold, the latching mechanism is switched by a bistable element to transmit power to the DoF that was previously locked and to lock the active one. In this case, the described behaviour translates into switching from grasping to twisting every time the gripper fingers' driving actuator requires torques larger than the threshold (e.g., the fingers are firmly grasping something or they reach the limit of their range of motion) and switching from twisting to grasping once the required torque is larger than the desired threshold (e.g., the twisting motion reached the desired screwing torque or the rotation is blocked by something). Fig. 1 depicts a simplified state machine diagram of the proposed gripper.

As anticipated before, to validate the general concept of a MRUM architecture, two different grippers are proposed here. The first proposed gripper is based on a 2-DoF epicyclic gearing architecture to enable both movements from a single input. Additionally, a bistable mechanism, paired with a ball-detent torque limiter, implements the torque-driven latching behaviour described above, allowing the transition between the two modes. As an alternative design, a ball-spline-based mechanism is proposed, capable of generating either linear or rotary output motion depending on the state of a bistable, torque-driven latch mechanism. In addition, a magnetic coupling is introduced as a design variant of the ball-detent torque limiter-based solution. The functional design of these elements is discussed in the next sections. However, note that the concept of MRUM can be extended beyond these two particular implementations, as different combinations of the already proposed subsystems can be designed or even different ones based on different transmissions (e.g., differential-based 2-DoF transmission) or different torque-driven multistable mechanisms.

2.1. Two-DoF transmission system

In general, any two-degree-of-freedom (2-DoF) transmission system that allows selective activation of one output while locking the other can serve as the basis for this gripper concept. Two possible implementations are presented here. The first employs an

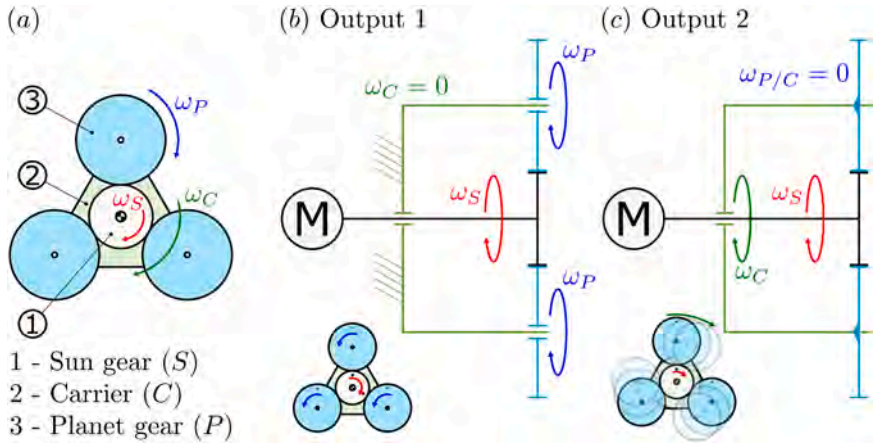

Fig. 2. Operating configurations of the proposed planetary gearing mechanism: (a) Diagram of the planetary gear; (b) *Output 1*: the carrier is fixed, and the system functions as an ordinary gear train transmitting motion from the sun gear (input) to the planet gears. (c) *Output 2*: the planet-carrier relative motion is constrained, and the carrier rotates, driven by the sun gear (input) in a manner equivalent to an external-internal gear pair.

epicyclic gear train, whereas the second utilises a compound ball-spline (also known as ball screw spline) mechanism to convert rotational input into either linear or rotary output motion.

2.1.1. *Epicyclic gear train*

A 2-DoF transmission is required to achieve the two desired motions from a single input. An epicyclic (planetary) gear system is one of these mechanical transmissions, where, considering the sun gear as input, the planets' rotation about their axis and the revolution of the whole planet carrier are the two alternative outputs, each one driving one of the two modes of operation.

Fig. 2 illustrates the two operating configurations. Fig. 2(a) shows a simplified representation of the epicyclic gear system. In Fig. 2(b), the carrier is locked, and the transmission operates as an ordinary gear pair, transmitting power from the sun gear (input) to the planet gears (*Output 1*). Conversely, in Fig. 2(c), the relative rotation between the planets and the carrier is constrained, while the carrier itself is free to rotate. In this configuration, the sun gear (input) transmits power to the carrier (*Output 2*), functioning analogously to an external gear (the sun gear) meshing with an internal gear (the carrier with locked planets).

The kinematic behaviour of the system can be described using the Willis equation:

$$\frac{\omega_{P/C}}{\omega_{S/C}} = \frac{\omega_P - \omega_C}{\omega_S - \omega_C} = i \tag{1}$$

Here, ω_S, ω_C, and ω_P denote the absolute angular velocities of the sun gear, carrier, and planet gears, respectively. The relative angular velocities are defined as $\omega_{P/C} = \omega_P - \omega_C$, representing the rotation of a planet gear with respect to the carrier, and $\omega_{S/C} = \omega_S - \omega_C$, representing the rotation of the sun gear with respect to the carrier. The parameter i is the characteristic transmission ratio, defined as

$$i = -\frac{z_S}{z_P} \tag{2}$$

where z_S and z_P are the numbers of teeth on the sun and planet gears, respectively.

In the *Output 1* configuration, the carrier is fixed ($\omega_C = 0$), and Eq. (1) simplifies to

$$\frac{\omega_P}{\omega_S} = i \tag{3}$$

which corresponds to the behaviour of an ordinary gear pair.

Conversely, in the *Output 2* configuration, the rotation of the planet gears about their own axes is constrained ($\omega_{P/C} = 0$, implying $\omega_P = \omega_C$). In this case, Eq. (1) reduces to

$$\omega_S = \omega_C = \omega_P \tag{4}$$

indicating that the carrier and sun gear rotate at the same angular velocity, regardless of the gear sizes or tooth numbers. Note that ω_P is nonzero: although the planets do not spin about their own axes, they still revolve around the carrier axis.

Table 2 summarises the operating configurations and their conditions.

Design-wise, it is irrelevant which output configuration (*Output 1* and *Output 2*) drives which mode (grasping mode or twisting mode). It mostly depends on how the actual gripper mechanism is designed. However, in the design proposed here, *Output 1* configuration drives the grasping mode and *Output 2* configuration controls the twisting mode.

Table 2
Operating configurations of an epicycloid gearing system and its kinematic relations.

	Output 1	Output 2
Sun gear	$\omega_S \neq 0$	$\omega_S \neq 0$
Carrier	$\omega_C = 0$	$\omega_C = \omega_S$
Planet gear	$\omega_P = i\omega_S$	$\omega_P = \omega_S$

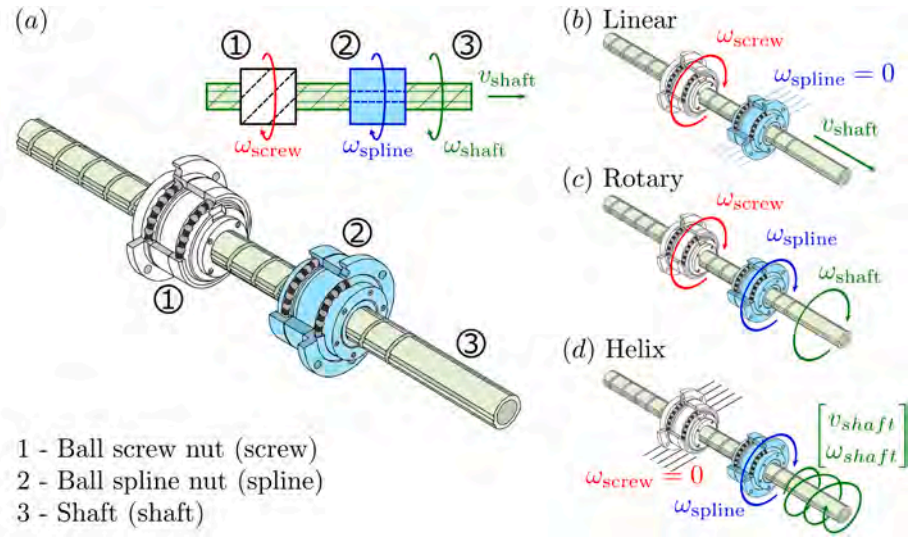

Fig. 3. Operating configurations of the proposed ball screw spline mechanism: (a) Diagram of the ball screw spline mechanism; (b) *Linear output*: the spline nut is fixed, and rotation of the screw nut drives the linear translation of the shaft. (c) *Rotary output*: the screw nut and spline nut rotate together at the same angular speed, causing the shaft to rotate at the same rate. (d) *Helix output*: the screw nut is fixed, and rotation of the spline nut drives a combined rotational and translational (helical) motion of the shaft.

Table 3
Operating configurations of a ball screw spline system and its kinematic relations.

	Linear output	Rotary output	Helix output
Screw nut	$\omega_{screw} \neq 0$	$\omega_{screw} \neq 0$	$\omega_{screw} = 0$
Spline nut	$\omega_{spline} = 0$	$\omega_{spline} = \omega_{screw}$	$\omega_{spline} \neq 0$
Shaft	$v_{shaft} = p\omega_{screw}$ $\omega_{shaft} = 0$	$v_{shaft} = 0$ $\omega_{shaft} = \omega_{screw}$	$v_{shaft} = p\omega_{spline}$ $\omega_{shaft} = \omega_{spline}$

2.1.2. Ball screw spline-based transmission

A ball screw spline combines two mechanical elements, namely a ball screw and a rotary ball spline, into a single integrated assembly. Therefore, it comprises three main components: a ball screw nut, a spline nut, and a shaft that features both a helical screw thread and longitudinal splines along its axis (Fig. 3(a)). This setup enables linear, rotary, or helical motion depending on which elements are driven (Fig. 3(b–d)).

When the ball screw nut is driven at an angular speed $\omega_{screw} \neq 0$ while the rotation of the spline nut is constrained ($\omega_{spline} = 0$), the shaft does not rotate ($\omega_{shaft} = 0$) and exhibits purely linear motion (*Linear output* configuration) with translational velocity

$$v_{shaft} = p\,\omega_{screw} \tag{5}$$

where p is the pitch of the screw.

Conversely, to obtain pure rotational motion of the shaft (*Rotary output* configuration), the screw nut and the spline nut are constrained to rotate together at the same angular speed ($\omega_{screw} = \omega_{spline}$). In this case, the shaft also rotates at the same rate,

$$\omega_{shaft} = \omega_{screw} = \omega_{spline} \tag{6}$$

Finally, when the ball screw nut is locked ($\omega_{screw} = 0$) and the spline nut is driven at an angular speed $\omega_{spline} \neq 0$, the shaft performs a combined rotational and translational motion, resulting in a helical motion (*Helical output* configuration). Specifically, the shaft rotates at $\omega_{shaft} = \omega_{spline}$ and translates with a linear velocity $v_{shaft} = p\,\omega_{spline}$.

Table 3 summarises the operating configurations and their corresponding conditions.

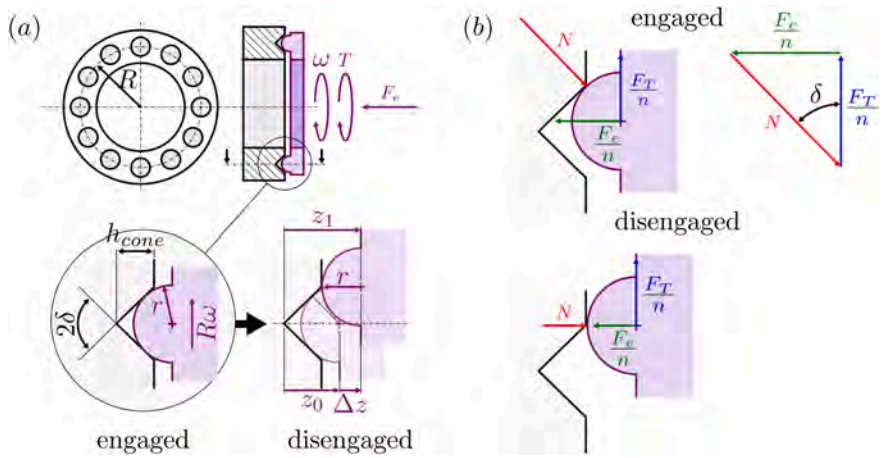

Fig. 4. Functional diagram of a ball-detent torque limiter. (a) Working principle and main parameters. (b) Free body diagram of one of the spheres while engaged and disengaged.

As mentioned before, for the planetary gear system, it is irrelevant which output configurations correspond to which gripper mode. For example, in the solution proposed here, the *Linear output* configuration drives the grasping mode, and the *Rotary output* configuration controls the twisting mode. The *Helix output* is not used.

2.2. Torque-driven bistable mechanism

In the previous section, it was shown that two distinct output motions can be obtained from a single input source. In general, this can be done by alternatively constraining one of the two possible output motions. In a fully actuated transmission, a dedicated actuator would control the selection of the desired output. However, in the present work, an underactuated approach is adopted to automatically switch between the two operating modes using a single source of motion.

As previously described and schematically shown in Fig. 1, a torque overload in the active transmission path can be interpreted as a mechanical signal indicating that a transition to the other operating mode is required. When such an overload occurs, the resulting reaction torque in the transmission should be high enough to release the constraint to the currently inactive mode, thereby activating it. At the same time, the torque overload also triggers a displacement of a bistable latching mechanism, which moves to its opposite stable configuration. This new configuration applies the constraint to the other output motion, locking the corresponding motion.

In summary, switching between grasping and twisting modes requires coupling the 2-DoF transmission with a torque-driven bistable latching mechanism. This kind of mechanism has two stable configurations, each corresponding to the constraint of one of the two possible modes of operation. When the applied torque exceeds the predefined torque threshold values, it triggers the whole mechanism. This removes the current constraint and shifts the bistable mechanism to the opposite configuration, imposing the constraint on the other mode of operation.

Two alternative design architectures are proposed here. The first solution features ball-detent torque limiters coupled with a bistable mechanism. The alternative design consists of a unique arrangement of face-to-face magnetic couplings to obtain the general behaviour described before. Both solutions, detailed in the next sections, are interchangeable with minimal changes to adapt the design to the chosen transmission system. However, here the ball-detent architecture is implemented in the epicyclic gear train, while the magnetic coupling is used in the solution centred around the ball screw spline mechanism.

2.2.1. Ball-detent torque limiter

Fig. 4 illustrates the operating principle of a typical ball-detent torque limiter (or clutch). The device consists of two disks facing each other: one features an array of n conical recesses with depth h_{cone} and half-angle δ, while the other carries n hemispherical detents of radius r (Fig. 4(a)). Both sets of features are positioned along a circle of radius R. An axial preload F_e, typically provided by an elastic element, presses the two disks together. A rotary input, defined by angular velocity ω and torque T, drives one of the disks.

When the spheres rest inside the conical recesses, the clutch is engaged, and the two disks rotate together as a single unit. As the applied torque T increases, the tangential component of the transmitted load causes the spheres to climb along the cone surfaces. If the torque remains below the threshold value, the clutch stays engaged, although the spheres are displaced from the rest position, but still within the cones. When the torque exceeds the threshold, the spheres are forced completely out of the recesses, and the clutch becomes disengaged, decoupling the two disks. Re-engagement occurs automatically once relative motion aligns the spheres with the next set of recesses.

As shown in Fig. 4(a), an axial displacement accompanies this transition. In the rest position (no torque applied), the centre of each sphere lies at an axial distance z_0 from the cone vertex, determined by the geometry of the cone and the sphere

$$z_0 = \frac{r}{\sin\delta} \tag{7}$$

When disengaged, the sphere lies outside the cone, with its centre at

$$z_1 = h_{cone} + r \tag{8}$$

Hence, the total axial displacement Δz between the engaged and disengaged configurations is

$$\Delta z = z_1 - z_0 = h_{cone} + r - \frac{r}{\sin\delta} = h_{cone} + r(1 - \frac{1}{\sin\delta}) \tag{9}$$

This displacement is particularly useful for triggering a bistable mechanism. During torque overload, the resulting disengagement of the clutch produces a sufficiently large axial motion to switch the bistable mechanism from one stable configuration to the other.

Fig. 4(b) shows the forces acting on each sphere-cone pair. Each sphere is pressed against the conical surface by an axial force F_e/n. The transmitted torque T, when evenly distributed among all n pairs, corresponds to a tangential force per sphere of

$$\frac{F_T}{n} = \frac{T}{nR} \tag{10}$$

When the clutch is engaged, the reaction force N at the contact point is normal to the cone surface and balances both the axial and tangential components. This leads to the relation between the transmissible torque and the applied axial force:

$$\frac{F_e}{n} = \frac{T}{nR}\tan\delta$$

or, for the entire clutch assembly,

$$F_e = \frac{T}{R}\tan\delta \tag{11}$$

The clutch remains engaged up to an axial displacement just before the maximum, Δz^-. At this point, the elastic element reaches its maximum compression, $F_e(\Delta z^-) = \max(F_e)$, allowing the torque overload threshold to be defined as

$$T_{thres} = \frac{RF_e(\Delta z^-)}{\tan\delta} \tag{12}$$

When disengaged, each sphere rests against the base of the cone, and the normal reaction N balances only the axial component F_e/n. The tangential component $\frac{F_T}{n}$, and consequently the torque, becomes unbalanced, allowing the two disks to slip freely without transmitting motion from the driven disk to the other.

As previously discussed, the 2-DoF transmission requires a mechanism that, when a torque overload is reached, produces a displacement large enough to trigger a bistable element and switch the output configuration. The ball-detent torque limiter serves this purpose effectively, as it allows the definition of a threshold torque T_{thres} based on the geometry of the sphere-cone pairs and the elastic axial load. When the transmitted torque exceeds T_{thres}, the detent disk moves axially by Δz. This displacement is sufficient to activate the bistable mechanism, which then drives the system toward its alternate stable configuration, engaging the opposite ball-detent clutch.

Fig. 5 illustrates this behaviour, where the bistable ball-detent torque limiter is integrated into the epicyclic gear train. The bistable mechanism consists of two sliders, B and C: slider B moves radially, while slider C moves axially, both relative to the planet carrier. The two sliders are connected by a rigid link BC, and an elastic element AB between the carrier and slider B completes the bistable assembly. The double-faced ball-detent disk is fixed to slider C, allowing it to shift axially between two sets of conical recesses–one attached to the fixed frame and the other to the planet gears.

Fig. 5(a) shows the *Output 1* configuration. Here, the ball-detent clutch sliding relative to the carrier is engaged with the frame, thereby constraining the carrier rotation ($\omega_C = 0$). In this condition, the transmission behaves as an ordinary gear train between the sun gear and the planets. If a dynamic event occurs that blocks the planet's rotation, a reaction torque exceeding the threshold T_{thres} develops at the carrier. This torque triggers the bistable ball-detent mechanism, causing slider C to move axially by Δz and surpass the unstable equilibrium position. The bistable mechanism then drives the motion to completion, engaging the opposite set of detents with the conical recesses fixed to the planet gears.

This new configuration, shown in Fig. 5(b), corresponds to *Output 2*. In this state, the rotation of the planets relative to the carrier is constrained ($\omega_{P/C} = 0$), so the sun gear drives the rotation of the entire carrier assembly, including the planets and the bistable clutch. Similarly, when the carrier's rotation is later blocked, and a new torque overload occurs, the bistable clutch fixed to slider C is again displaced, re-triggering the bistable mechanism and restoring the *Output 1* configuration.

The functional mechanism shown in Fig. 5 employs a typical discrete element bistable mechanism. However, it is of great interest to implement a compliant equivalent mechanism to achieve the same behaviour with the least amount of elements. In the next section, a bistable curved beam is introduced as an alternative.

Bistable curved beams

Clamped-clamped curved beams are a typical monolithic implementation of bistable mechanisms [16]. Fig. 6 illustrates a pre-shaped curved beam, showing its main geometric parameters: thickness t, length l, and initial height h. The curved beam also has a depth b, not shown in the figure.

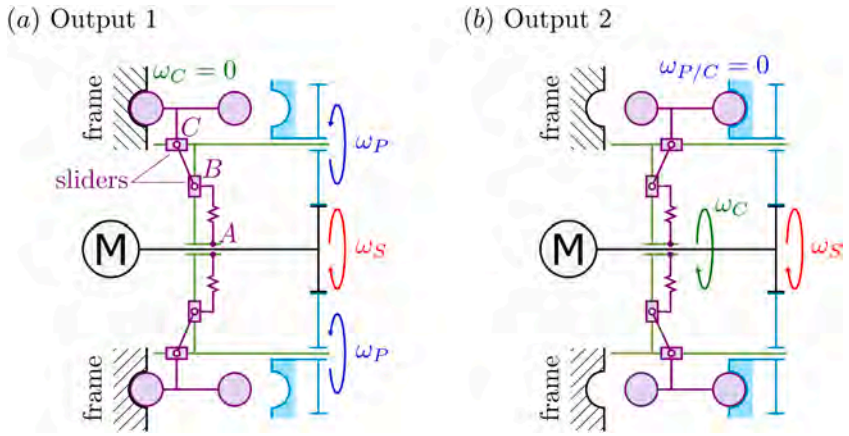

Fig. 5. Functional diagram of the bistable ball-detent torque limiter integrated in the epicyclic gear train to select one of the outputs. (a) *Output 1*: the ball-detent is engaged with the frame, constraining the carrier rotation. (b) *Output 2*: the planet rotation relative to the carrier is constrained by the ball-detent engaging with the planets.

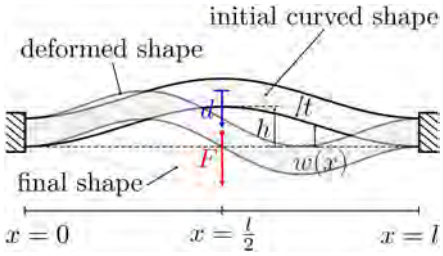

Fig. 6. Clamped-clamped curved bistable beam at its initial, intermediate, and final positions during the transition between stable configurations.

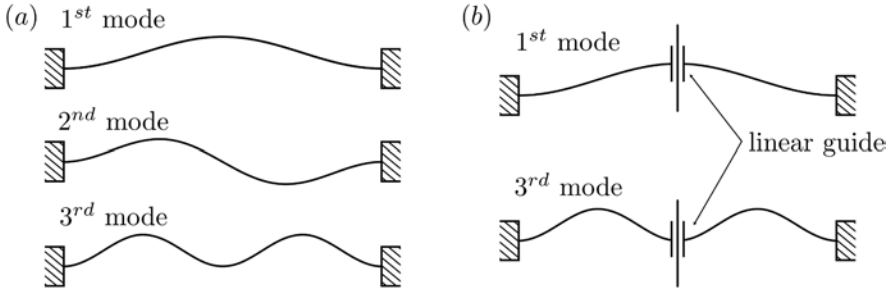

Fig. 7. (a) Main modes of deformation of a clamped-clamped curved beam. (b) Example solution to avoid the second buckling mode by adding a linear guide at the beam centre.

The initial shape of the beam resembles the first buckling mode of an axially compressed buckling beam:

$$w(x) = \frac{h}{2}\left(1 - \cos\left(2\pi\frac{x}{l}\right)\right); \tag{13}$$

Previous studies demonstrated that a curved beam exhibits a bistable behaviour under a force F or a displacement d only when the height-to-thickness ratio $Q = h/t$ is greater than 2.31 [16,17], although in practice significantly higher values are employed. During the transition between its stable positions, the beam passes through different buckling modes, in particular the first three (Fig. 7(a)). Notably, the odd buckling modes are symmetric, whereas the second buckling mode is asymmetric and thus typically undesired. To avoid such behaviour, two curved beams are paired and connected at their centres, or a linear slide can be added at the beam midpoint to constrain the beam deformation (Fig. 7(b)).

Hussein et al. in Hussein et al. [18] provided a design method for bistable curved beams to obtain the desired force-displacement characteristic. Referring to Fig. 8, which depicts the typical force-deformation characteristics of a bistable beam, the main parameters can be defined as:

$$d_0 = 0; \tag{14}$$

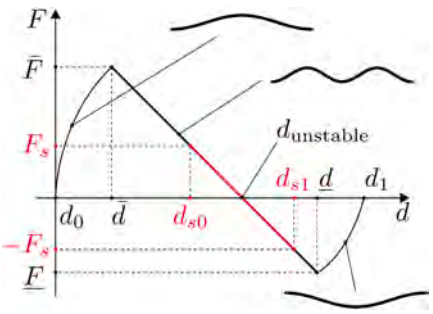

Fig. 8. Force-deformation characteristic of a bistable curved beam.

$$d_{\text{unstable}} = \frac{4}{3}h \tag{15}$$

$$d_1 = \left(\frac{3}{2} + \sqrt{\frac{1}{4} - \frac{4}{3Q^2}}\right)h \tag{16}$$

where d_0 and d_1 are the two stable equilibrium points, while d_{unstable} is the unstable one, defining the transition point between the two stable configurations.

Before snapping from one stable configuration to the other, the beam reaches two peak forces, $\bar{F}$ and $\underline{F}$, corresponding to the positive and negative extremes:

$$\bar{F} = \frac{32\pi^2}{9}\frac{Ebt^3h}{l^3}\left(\frac{4}{9} + \pi\sqrt{\frac{1}{6} + \frac{16}{81\pi^2} - \frac{1}{Q^2}}\right) \tag{17}$$

$$\underline{F} = \frac{32\pi^2}{9}\frac{Ebt^3h}{l^3}\left(\frac{4}{9} - \pi\sqrt{\frac{1}{6} + \frac{16}{81\pi^2} - \frac{1}{Q^2}}\right) \tag{18}$$

where E is the Young's modulus of the material. These two peak forces occur, respectively, at the following deflections

$$\bar{d} = \left(\frac{28}{27} - \frac{2}{3}\pi\sqrt{\frac{1}{6} + \frac{16}{81\pi^2} - \frac{1}{Q^2}}\right)h \tag{19}$$

$$\underline{d} = \left(\frac{28}{27} + \frac{2}{3}\pi\sqrt{\frac{1}{6} + \frac{16}{81\pi^2} - \frac{1}{Q^2}}\right)h \tag{20}$$

Initially, the snapping force increases with deflection, dominated by the first buckling mode, until the displacement $\bar{d}$ is reached. Between $\bar{d}$ and $\underline{d}$, the third buckling mode dominates, resulting in a constant negative-stiffness region. Beyond $\underline{d}$, the third mode no longer contributes, and the stiffness returns positive. The negative stiffness between $\bar{d}$ and $\underline{d}$ leads to bistability.

The resulting force-deformation characteristic is clearly not symmetric about the unstable equilibrium point, either in force magnitude or displacement. However, for many applications, a symmetric behaviour is preferable or even required.

A practical approach to achieve this symmetry is to employ stop-blocks to limit the deflection within the linear zone around d_{unstable}. In particular, given a desired stroke d_s centred around the unstable position, the two stop-blocks must limit the deflection between the positions

$$d_{s0} = \frac{4}{3}h - \frac{1}{2}d_s \tag{21}$$

$$d_{s1} = \frac{4}{3}h + \frac{1}{2}d_s \tag{22}$$

resulting in an elastic force at both the stop-block equal to

$$|F_s| = \frac{8}{3}\pi^2\frac{Ebt^3}{l^3}d_s \tag{23}$$

When coupled with the ball-detent clutch, the elastic force F_e keeping the two disks of the clutch in contact corresponds to the reaction force F produced by the bistable beam. Hence, the overload torque is related to the maximum force exerted by the bistable beam

$$T_{thres} = \frac{R}{\tan\delta}F_s \tag{24}$$

Similarly, since the detent displacement drives the beam deflection, triggering the transition between the stable configurations requires that

$$\Delta z \geq \frac{d_s}{2} \tag{25}$$

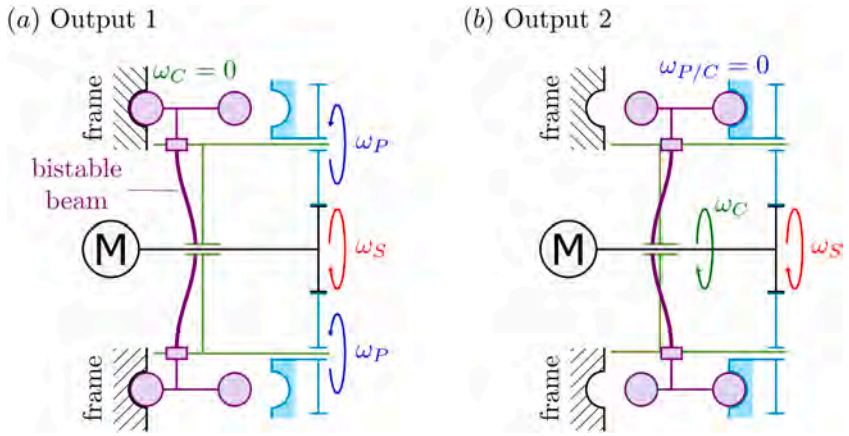

Fig. 9. Functional diagram of the ball-detent torque limiter with a monolithic bistable element integrated in the epicyclic gear train to select one of the outputs. (a) *Output 1*: the ball-detent is engaged with the frame, constraining the carrier rotation. (b) *Output 2*: the planet rotation relative to the carrier is constrained by the ball-detent engaging with the planets.

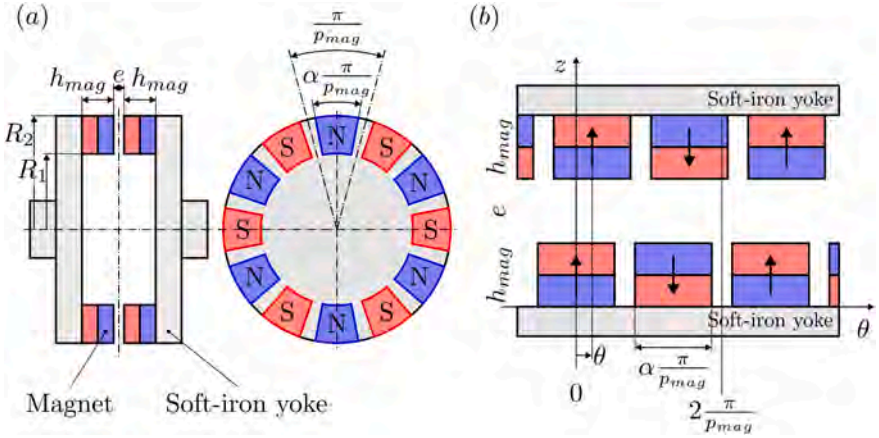

Fig. 10. (a) Schematic representation of the face-to-face magnetic coupling. (b) Net view of the magnetic coupling at the average radius $R_e = (R_1 + R_2)/2$.

Fig. 9 presents the functional diagram of the complete system, where the monolithic bistable element is integrated with the ball-detent torque limiter within the two-DoF epicyclic gear train.

The main difference between this new configuration and the one shown in Fig. 5 is that the bistable mechanism made of the two sliders B and C linked together, and the elastic element AB has been replaced by the pre-curved beam.

It is important to note that the beam operates in a kinematically inverted manner compared with the standard case: the beam ends move while the midpoint remains fixed. To achieve this, the beam centre is constrained to rotate together with the carrier, which also suppresses the undesired second buckling mode. The two beam ends, on the other hand, can slide axially, performing a role analogous to that of slider C in the previous configuration.

2.2.2. Magnetic coupling

An alternative solution to the bistable ball-detent torque limiter can be achieved by employing a face-to-face magnetic coupling. This type of coupling consists of two coaxial disks facing each other, each embedding an array of $2p_{mag}$ permanent magnets, where p_{mag} is the number of pole pairs, arranged with alternating polarities along a circular pattern (Fig. 10). The magnets on the driving and driven disks interact magnetically, enabling torque transmission without mechanical contact.

Fig. 10 also defines the main geometric parameters of the coupling, namely inner and outer magnet radii R_1 and R_2, the air gap e, and the magnet thickness h_{mag}. The ratio between the magnet arc length and maximum available arc length due to the number of pole pairs (pole pitch ratio) is defined as α. Under dynamic loading, an angular displacement θ occurs between the two disks, affecting the magnetic field. Such displacement is typically due to the transmitted torque; thus, it is also known as the torque angle or slip angle.

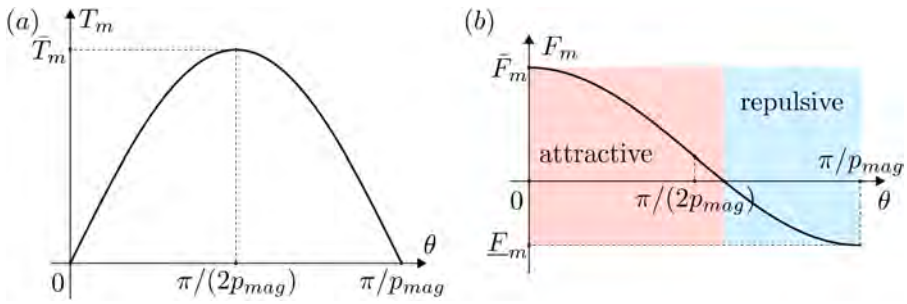

Fig. 11. Qualitative characteristics of the magnetic coupling (a) Magnetic torque T_m as a function of the angular displacement θ. (b) Magnetic axial force F_m as a function of the angular displacement θ.

Lubin et al. [19] provided closed-form expressions for the magnetic axial force and torque. The magnetic torque can be represented with good approximation by the following relation:

$$T_m = \frac{16}{3\pi}\frac{B_r^2}{\mu_0}R_2^3\left(1-\left(\frac{R_1}{R_2}\right)^3\right)\sin^2\left(\alpha\frac{\pi}{2}\right)\frac{\sinh^2\left(p_{mag}\frac{h_{mag}}{R_e}\right)}{\sinh\left(2\left(1+\frac{e}{2h_{mag}}\right)p_{mag}\frac{h_{mag}}{R_e}\right)}\sin(p_{mag}\theta) \tag{26}$$

where B_r is the remanence of the magnets, μ_0 is the permeability of the vacuum, and $R_e = (R_1 + R_2)/2$ is the mean radius of the magnets.

Similarly, the corresponding axial force is:

$$F_m = \frac{8}{\pi}\frac{B_r^2}{\mu_0}R_2^2\left(1-\left(\frac{R_1}{R_2}\right)^2\right)\sin^2\left(\alpha\frac{\pi}{2}\right)\frac{\sinh^2\left(p_{mag}\frac{h_{mag}}{R_e}\right)}{\sinh\left(2\left(1+\frac{e}{2h_{mag}}\right)p_{mag}\frac{h_{mag}}{R_e}\right)}\left(\cos(p_{mag}\theta)\cosh\left(2\left(1+\frac{e}{2h}\right)p_{mag}\frac{h}{R_e}\right)+1\right) \tag{27}$$

As reported by Lubin et al. [19], this closed-form method is simpler but lacks accuracy compared to 3D numerical simulations, yet it is able to provide a useful tool for an initial sizing of the subsystem. Therefore, a proper 3D numerical simulation is required to obtain the most accurate model of the magnetic coupling, but this simplified analytical model is enough to obtain close-to-optimal parameters, such as the number of pole pairs or the general sizing.

The qualitative behaviour of T_m and F_m as functions of θ is shown in Fig. 11(a) and (b), respectively.

At rest ($\theta = 0$), magnets with opposite polarity face each other, resulting in the maximum attractive axial force F_m and zero transmitted torque T_m. As the driving torque increases, the angular slip θ grows, causing progressive misalignment between the magnets of the facing disks. Consequently, the attractive axial force decreases while the transmissible torque increases. The transmissible torque reaches its peak at half the pole pitch ($\theta = \pi/(2p_{mag})$), which defines the full-load condition. The axial force is still slightly attractive, and it becomes zero for an angle slightly higher than half the pole pitch. Beyond this point, the axial force becomes repulsive ($F_m < 0$) and rises in magnitude while the transmissible torque decreases. At $\theta = \pi/p_{mag}$, the system reaches an unstable condition where magnets of equal polarity face each other, producing the maximum repulsive force (the magnetic axial force reaches its minimum) and null transmissible torque.

This magnetic behaviour can be exploited to realise a torque-driven bistable mechanism within the ball screw spline transmission (Fig. 12). Compared to the previously described magnetic coupling, the whole system is doubled with a total of four disks with an array of magnetic poles. The central pair forms a translating shuttle that can move axially. During normal operating conditions, the moving shuttle is magnetically coupled with one of the two disks. When the driving torque exceeds the maximum transmissible torque, the slip angle increases beyond the full-load condition, causing the axial magnetic force to become repulsive. This force pushes the shuttle away, weakening the magnetic coupling with the current disk and strengthening it with the other one. If the axial displacement is sufficient, the shuttle snaps to the other side, establishing the magnetic coupling with the other disk.

Fig. 12 also shows how this bistable mechanism is implemented in the ball screw spline transmission. A magnetic disk is fixed to the screw nut facing the spline nut. The ball spline nut acts as the shuttle with two magnetic disks described before. Finally, the last magnetic disk is fixed to the frame to the right of the spline nut. When the ball spline nut is coupled with the frame, its rotation is constrained, and the screw nut produces a pure translation of the shaft (*Linear output*, Fig. 12(a)). On the contrary, when the screw nut and the spline nut are magnetically coupled, they rotate at the same speed, causing the rotation of the shaft (*Rotary output*, Fig. 12(b)).

2.3. Gripper mechanism

The design of the gripper mechanism is not subject to strict constraints or requirements. It primarily depends on how the 2-DoF transmission system can alternately produce the motions required for twisting and grasping. Naturally, specific design requirements are also determined by the characteristics of the objects to be manipulated. Two simple and minimalistic gripper solutions are presented here, each tailored to one of the two proposed transmission mechanisms.

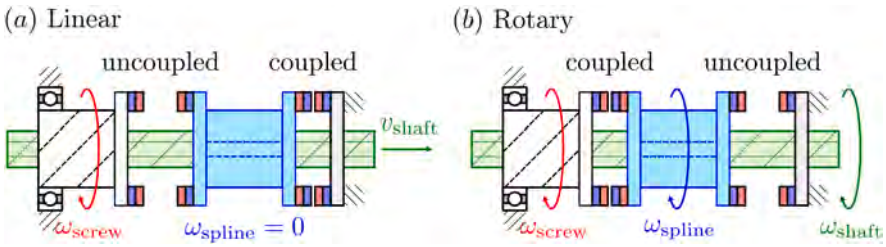

Fig. 12. Implementation of the magnetic coupling in the ball screw spline mechanism to achieve the desired bistable behaviour. (a) *Linear output*: the spline nut is fixed because it is coupled with the frame, and rotation of the screw nut drives the linear translation of the shaft. (b) *Rotary output*: the screw nut and spline nut rotate together at the same angular speed thanks to the magnetic coupling, causing the shaft to rotate at the same rate.

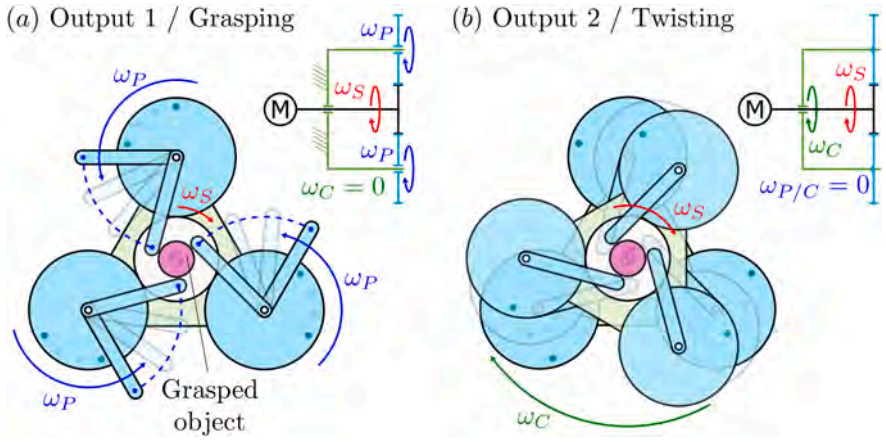

Fig. 13. Functional diagram of the gripper for the epicyclic gear train. The bistable mechanism is not shown for clarity. (a) *Output 1/Grasping*: each finger, rigidly attached to a planet gear, rotates about its own axis to produce a radial grasping motion. (b) *Output 2/Twisting*: the rotation of the planet gears relative to the carrier is constrained, causing the planets and their fingers to rotate with the carrier, twisting the grasped object.

2.3.1. *Gripper design for the epicyclic gear train*

The first design is made for the epicyclic gear train mechanism and is schematically illustrated in Fig. 13. A rotating finger is rigidly attached to each planet gear such that, when the planet gears rotate about their own axes (*Output 1* configuration), a sort of radial grasping motion is produced (Fig. 13(a)). Conversely, when this rotation is constrained, the entire carrier rotates (*Output 2* configuration), causing the gripper, and thus the fingers mounted on the planet gears, to rotate about the central axis of the transmission without releasing the grasped object (Fig. 13(b)).

Due to its design, this kind of gripper is particularly suited for manipulation tasks involving axially symmetric objects.

2.3.2. *Gripper design for the ball screw spline mechanism*

The second design is conceived for more general-purpose manipulation tasks, enabling the grasping of objects with varied shapes. Fig. 14 shows the functional diagram of this gripper. The *Linear output* motion generated by the ball screw spline mechanism drives the fingers' grasping motion through a simple linkage mechanism (Fig. 14(a)). The link A_0A_1 is hinged at A_0 to the shaft, while the link $A_1B_0B_1$, being the actual gripper finger, is hinged at B_0 to a revolute joint whose axis is the same as the whole transmission. When the transmission operates in the *Rotary output* configuration, and thus the output shaft is only rotating, the twisting motion of the whole gripper is achieved thanks to the added revolute joint (Fig. 14(b)).

2.4. *Key parameters and design guidelines*

To bridge the gap between the analytical models presented in Section 2 and the practical implementation of the prototypes, a cohesive design procedure is proposed. This workflow ensures that the chosen torque thresholds, bistable elements, and transmission geometries are mutually compatible and tailored to the target manipulation task. Yet, it is important to note that the concept of a MRUM-based gripper is not limited to the two proposed prototypes; therefore, the design guidelines proposed here are mostly meant to highlight how the different parameters and design choices are linked together.

The design of a MRUM follows a structured five-step sequence:

1. **Establish Task-Specific Requirements:** The procedure begins by defining the torque (or force) requirements of the intended application. This involves identifying the resistance of the object to be manipulated (e.g., the cracking torque of a valve or the friction of a screw) to set a baseline for the transition thresholds.

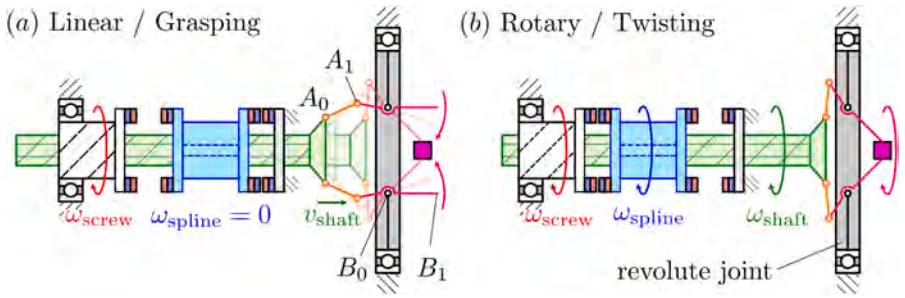

Fig. 14. Functional diagram of the gripper for the ball screw spline transmission. (a) *Linear/Grasping*: a gripper consisting of a linkage mechanism is driven by the linear motion of the shaft. (b) *Rotary/Twisting*: the rotating shaft makes the whole gripper rotate, twisting the grasped object.

2. **Architectural Design of the 2-DoF Transmission:** The 2-DoF transmission is designed by considering its two degrees of freedom independently. This includes selecting the appropriate architecture, such as an epicyclic gear train, a ball screw spline or a different 2-DoF transmission, and determining the transmission ratios (i or p) required to convert the single actuator input into the desired grasping and twisting outputs.
3. **Selection and Adaptation of the Latching Mechanism:** A torque-driven latching mechanism is selected and adapted to the requirements defined in the previous steps. Whether employing a mechanical ball-detent, a contactless magnetic coupling or even a different one, the physical principle must be compatible with the transmission's geometry and the environmental conditions of the task.
4. **Sizing of the Bistable Element and Threshold Tuning:** The results of the previous step are refined by relating the desired threshold torque (T_{thres}) to the latch mechanism's maximum transmissible torque. The bistable element (e.g., a curved beam or the magnetic coupling) is then sized to trigger at this specific threshold, accounting for any intermediate transmission ratios. This involves balancing the latching force (F_s or F_m) required to maintain a stable state with the necessity for the latching displacement to be sufficient to overcome the mechanism's unstable equilibrium point. Note that in the case of using a ball-detent torque limiter or similar contact-based mechanism, the displacement is geometrically defined ($\Delta z \geq d_s/2$). If the magnetic couplings are used instead, it is less straightforward to define a displacement geometrically, but generally speaking, it is possible to produce a significant displacement whenever the axial magnetic field of the opposing disks and the shuttle are strong enough.
5. **Iterative Revision and Finalisation :** Finally, the various subsystems are cross-referenced to ensure global compatibility. For instance, the stiffness of the bistable beam must be reconciled with the available volume within the transmission housing, and the resolution of the detents must be checked against the desired grasping precision. This iterative process ensures that the autonomous switching logic remains robust under varying operational speeds and accelerations.

2.5. Design case example

To illustrate the practical application of the proposed design guidelines, this section outlines a step-by-step sizing procedure for a MRUM-based gripper. Consider a scenario where a manual valve requires an operational torque $T_{valve} = 0.1\,\text{Nm}$ to be opened or closed. The system design must ensure that the switching torque threshold T_{thres} is sufficiently higher than T_{valve} to guarantee robust, repeatable latching behaviour while avoiding premature mode switching.

If a magnetic coupling is selected, (26) can be employed for initial sizing. Assuming the use of two opposing disks, each featuring $2p_{mag} = 20$ cylindrical magnets (diameter 3 mm, height $h_{mag} = 2\,\text{mm}$) with remanence $B_r = 1\,\text{T}$, placed at a radius $R_e = 12.5\,\text{mm}$, with a pole pitch ratio $\alpha \approx 0.65$ and a gap $e = 1\,\text{mm}$, the maximum holding torque (at an angular displacement $\theta = \pi/(2p_{mag})$) is estimated as:

$$T_{thres} = \overline{T}_m \approx 0.29\,\text{Nm} \tag{28}$$

Although (26) typically provides an upper-bound estimate, this value serves as a conservative threshold that ensures the gripper transitions to the twisting mode only after the valve has been securely grasped, thereby accounting for unmodeled system losses, such as transmission efficiency.

Defining the automatic mode switching from grasping to twisting is more complex, as it involves the coordination of multiple design parameters. To define a requirement for this phase, the required operational torque has to be related to the gripper's normal force. Assuming a friction coefficient between the fingers and the valve knob of $\mu_{valve} = 0.5$ and an external knob diameter $OD = 30\,\text{mm}$, the required normal force N_{valve} is:

$$N_{valve} = \frac{2T_{valve}}{OD \cdot \mu_{valve}} \approx 13.33\,\text{N} \tag{29}$$

This force requirement dictates the necessary input torque at the transmission stage. Assuming a ball-screw spline transmission with a screw pitch $p = 5\,\text{mm}$ and a unitary transmission ratio for the finger mechanism, the corresponding input torque T_{grip} is computed as:

$$T_{grip} = p \cdot N_{valve} \approx 0.067\,\text{Nm} \tag{30}$$

Table 4
Design parameters for the epicyclic gear prototype.

Subsystem	Parameter	Value	Parameter	Value
Transmission	Sun gear teeth z_S	16	Planet teeth z_P	32
	Module	1.5	Helix angle	40°
	Pressure angle	20°		
Torque Limiter	Radius R	29 mm	Detent radius r	3.5 mm
	Recess depth h_{cone}	4.04 mm	Half angle δ	60°
	Ball-detent resolution	8	Ratchet angle	60°
	Ratchet resolution	24	Height	3.5 mm
Bistable Beam	Length l	82 mm	Width b	20 mm
	Thickness t	1 mm	Pre-shaped height h	3.5 mm

The calculated threshold ($T_{thres} = 0.29$ Nm) is significantly higher than the required input torque ($T_{grip} = 0.067$ Nm), confirming that the magnetic coupling design is appropriate for both operational modes, which simplifies the overall assembly. Note that the actual driving torque could be much larger due to the low efficiency of screw transmission, while the actual threshold value is generally overestimated by the model used to compute it

Finally, it should be noted that, while this example provides a starting point, an iterative design process is typically required to refine these parameters and ensure optimal performance in a final prototype.

3. Prototypes design

Two prototypes were assembled to validate the concepts previously described. No particular requirements or constraints were imposed on the design since the desired result was building two working prototypes to validate the working principle. This allowed to fabricate most of the two prototypes by additive manufacturing, in particular using PLA. The details of each prototype are reported in the next sections.

3.1. Epicyclic gear gripper

The first prototype is based on the epicyclic gear gripper described before. The final design is shown in Fig. 15(a) as a section view of the CAD model and as the assembled prototype in Fig. 15(b).

The planetary gear set consists of a double-helical sun gear with $z_S = 16$ teeth meshing with three double-helical planet gears, each having $z_P = 32$ teeth. All gears share a module of 1.5, a helix angle of 40°, and a pressure angle of 20°.

The ball-detent torque limiter between the gripper frame and the bistable subsystem shuttle is composed of two mating parts: one fixed to the frame and featuring 12 conical recesses, and one fixed to the shuttle carrying 12 hemispherical detents. The detents and recesses are arranged along a circumference of radius $R = 29$ mm. The cone recesses have a depth of $h_{cone} = 4.04$ mm and a half-angle $\delta = 60°$. The spheres have a diameter of $2r = 7$ mm. When engaged and at rest, the centre of each sphere lies at the base of the corresponding cone.

Initially, similar ball-detent torque limiters were employed between each planet gear and the bistable shuttle. In this configuration, the detent and recess dimensions were unchanged, but the number was limited to 8 along a circumference of radius $R = 19$ mm. However, preliminary tests revealed that this solution revealed significant synchronisation issues during transitions between the two operating stages, mostly because of the limited angular resolution due to the limited number of detents. Therefore, to address this issue, the ball-detents clutch was replaced by a face-engaging ratchet clutch with 24 sawtooth detents, each with an inclination of 60° and a height of 3.5 mm, within the same volume of the original ball-detent torque limiter. This modification significantly improved synchronisation during mode transition at the cost of making the torque limiter unidirectional. For the specific valve-turning task presented in this work, this lack of bidirectionality was functionally irrelevant, as the task did not require a torque-triggered transition in the ratchet's locked direction. While this is generally acceptable, there may be some specific applications where a bi-directional torque limiter may be required. In those scenarios, a ball-detent with a high number of detents would be necessary, implying a larger clutch with small detents and consequent implications for both the overall size and the bistable element design.

The bistable subsystem was completed by a spring steel strip used as a bistable beam. The strip is $l = 82$ mm long, $b = 20$ mm wide, and with thickness $t = 1$ mm. The beam is axially compressed to obtain a deformed shape with a height of $h = 3.5$ mm. The axial preload, and thus the beam deformation, can be regulated by a mechanism similar to a conical coupling, where by tightening or loosening a threaded cap, the axial displacement of the beam can be increased or decreased thanks to opposing conical surfaces.

The gripper was realised by rigidly attaching a 55 mm long finger to each planet gear. The fingers were padded with a strip of Scotch-Brite to increase friction during grasping.

The complete prototype had an outer diameter of about 160 mm (with the fingers remaining within the frame envelope) and an overall height of 88 mm. The total mass of the assembly is about 368 g.

The primary technical specifications for the epicyclic gear prototype are summarised in Table 4. These parameters define the mechanical transmission ratios, the switching thresholds of the torque-driven latch, and the structural dimensions of the bistable beam.

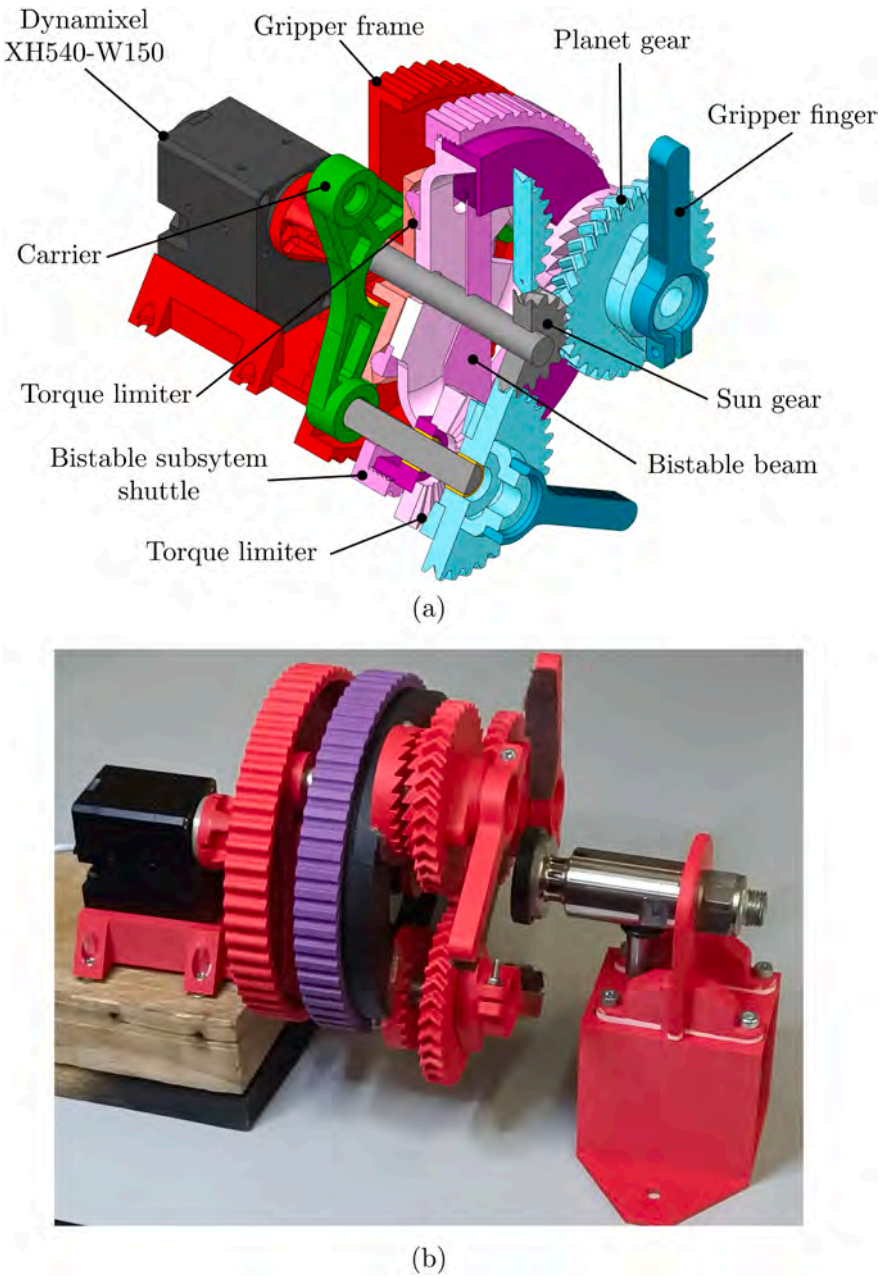

Fig. 15. Design of the gripper based on the epicyclic gear transmission. (a) CAD view of the designed prototype. (b) Gripper prototype on the test bench.

3.2. Ball screw spline gripper

The second prototype is based on the ball screw spline gripper. The final design is shown in Fig. 16(a) as a section view of the CAD model and as the assembled prototype in Fig. 16(b).

The system is driven by a ball screw nut meshing with a screw shaft with a diameter of 10 mm. Both components feature a helical screw thread with a pitch $p = 5$ mm. Moreover, the shaft has 6 longitudinal grooves along its axis to engage with the ball spline nut. All grooves and the screw thread are sized to accommodate spheres with a diameter of 2 mm.

The ball screw nut and the ball spline nut feature, on their opposing faces, the first magnetic coupling used as the bistable torque-driven latch mechanism. In particular, the magnetic coupling is composed of $p_{mag} = 10$ magnetic pole pairs per coupling arranged along a circumference of radius $R_e = 12.5$ mm. The magnets are cylindrical neodymium magnets with a diameter of 3 mm and a height of $h_{mag} = 2$ mm. They are N35-grade axially magnetised cylinders with a surface magnetic flux density of about 1 T and an adhesive

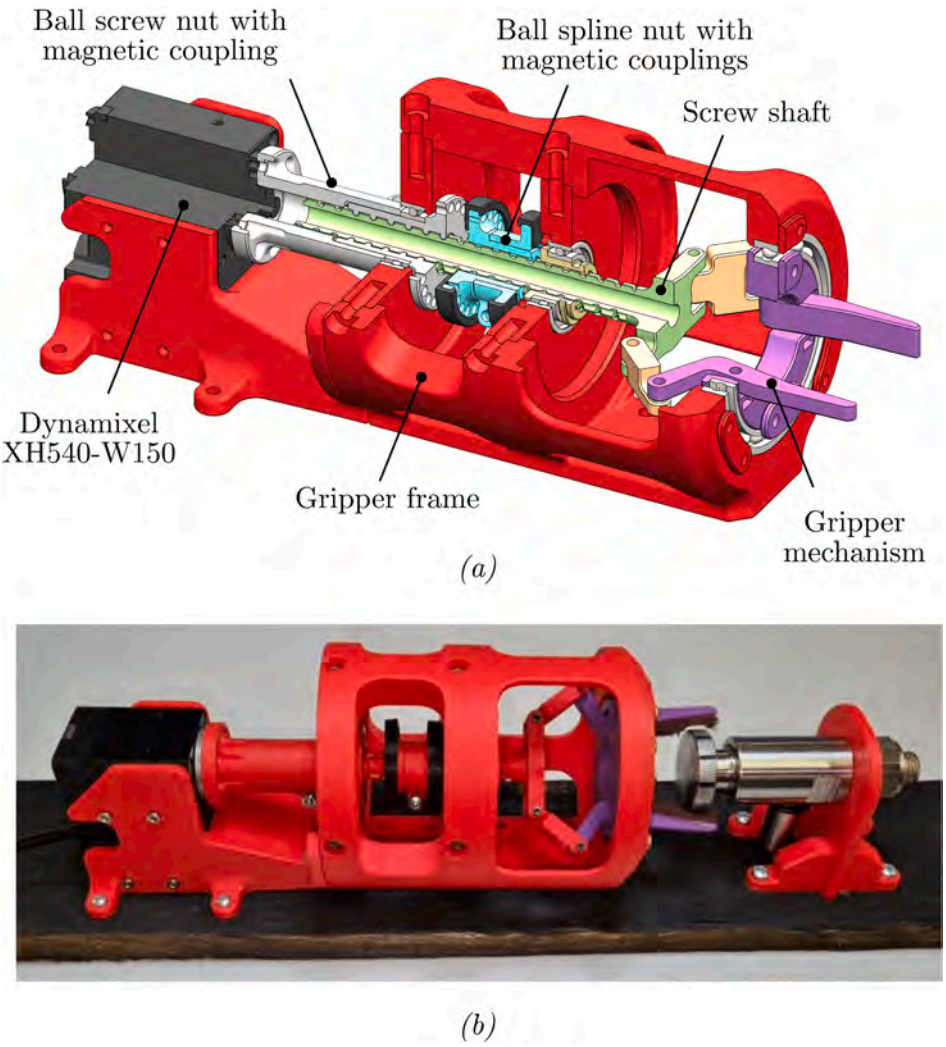

Fig. 16. Design of the gripper based on the ball screw spline transmission. (a) CAD view of the designed prototype. (b) Gripper prototype on the test bench.

Table 5
Design Parameters for the ball screw spline prototype.

Subsystem	Parameter	Value	Parameter	Value
Transmission	Shaft diameter	10 mm	Screw pitch p	5 mm
	Spline grooves	6	Ball diameter	2 mm
Magnetic Latch	Pole pairs p_{mag}	10	Mean radius R_e	12.5 mm
	Magnet type	N35 neodymium	Dimensions (D×H)	3 mm×2 mm
	Screw spline air gap	1 mm	Frame air gap	0.5 mm
Gripper	Link A_0A_1	20 mm	Link B_0A_1	20 mm

force 2.4 N. When the two faces are magnetically coupled and at rest, the air gap between them is $e = 1$ mm. The magnetic coupling between the ball spline nut and the gripper frame is identical in design, except that the air gap when coupled is $e = 0.5$ mm instead.

In the gripper mechanism, links A_0A_1 and B_0A_1 both have a length of 20 mm.

The complete prototype has an outer diameter of 86 mm and an overall height of 140 mm. The total mass of the assembly is approximately 283 g.

For the ball screw spline prototype, the key parameters governing the transmission and the magnetic latching thresholds are detailed in Table 5.

4. Experimental validation

A simple experimental campaign was done to validate the concept of the two prototypes by demonstrating that they were able to transition between modes in a possible use-case scenario, such as opening and closing a valve. The next section reports the experimental methodology, while later the results for both prototypes are shown and discussed.

4.1. Experimental setup

The objective of the experimental tests was to demonstrate that the two assembled prototypes can open and then close a valve automatically, transitioning between grasping and twisting modes, and vice versa, to validate the general concept presented here.

A manual valve used for wine sampling during the fermentation and refinement phases was used as the test valve. Specifically, the valve knob is intended for manual operation and has an outer diameter of 30 mm. The valve opens and closes proportionally by loosening and tightening the threaded knob. For testing the grippers, the valve was mounted on a dedicated support and placed in front of the gripper at such a distance that the fingers were able to grasp and rotate the knob.

A Dynamixel XH540-W150 servo-motor was used to drive the input shaft of both prototypes. The motor was controlled in position, first to grasp and open the valve (clockwise input rotation in the motor reference frame) and then to close and release the valve (anticlockwise input rotation in the motor reference frame). Specifically, the motor was commanded to reach a defined angular displacement following a trapezoidal velocity profile (valve opening phase) and then go back to the starting position, always constrained by the trapezoidal velocity profile (valve closing phase). The velocity profiles were adapted to the two different prototype transmissions. In particular, for the epicyclic gear gripper, the motor was commanded to rotate 600° clockwise and then return to the starting position under the constraint of a trapezoidal velocity profile with a maximum angular acceleration of $85\,\mathrm{deg/s^2}$ and a maximum angular speed of $50\,\mathrm{deg/s}$. Instead, for the ball screw gripper, the angular displacement was 1000° with a maximum angular acceleration of $22\,\mathrm{deg/s^2}$ and a maximum angular speed of $68\,\mathrm{deg/s}$. The differences in profile were used only to better adapt to the different prototypes.

During each test run, the angle and the motor current were measured by the motor controller. The motor torque was computed from the current using the torque constant $k_T = 1.2\,\mathrm{Nm/A}$ provided by the motor manufacturer. The constant already considers the servo-motor gear ratio. Note that this measurement represents the torque at the motor output (before the 2-DoF transmission) and that external frictional losses and transmission efficiency were neglected in this characterisation.

The valve opening and closing test was repeated ten times for each prototype, every time with an initial random orientation of the gripper and its finger. The experimental setups for the two prototypes are shown in Figs. 15(b) and 16(b).

5. Results

Fig. 17 illustrates one of the functionality tests done with the epicyclic gear gripper. At the beginning of the test, the motor rotated clockwise (negative angular speed), causing the fingers to close and grasp the valve knob (*grasping* mode). At about 2.9 s the motor torque peaked after the knob was firmly grasped. This torque overload triggered the automatic transition to the *twisting* mode, resulting in the gripper loosening the valve knob. At 12.77 s, the motor reached the commanded angular displacement and began returning to the initial position by rotating anticlockwise (positive angular speed). As a result, the gripper, still holding the knob, began tightening the valve. At 26.64 s, the motor torque peaked again as the valve was fully closed. This second torque overload caused the bistable clutch to switch back to the *grasping* mode, leading to the opening of the gripper fingers and the release of the valve.

The experimental campaign for both prototypes yielded a 100% success rate, with each device successfully completing 10 out of 10 trials for the full valve opening and closing sequence. The autonomous transitions occurred consistently without any instances of missed switches or permanent mechanical jams.

Considering all tests conducted with the epicyclic gear gripper, the mean maximum torque (i.e., the torque triggering the transition from tightening the knob to releasing the grasp) was $0.323 \pm 0.047\,\mathrm{Nm}$. Similarly, the mean minimum torque (i.e., the torque triggering the transition from grasping the knob to loosening it) was $-0.364 \pm 0.070\,\mathrm{Nm}$. This switching torque corresponds to an estimated peak grasping force of about $13.2 \pm 2.55\,\mathrm{N}$, providing a consistent grip before the transition to twisting occurs. This estimate has been computed considering that the fingers are 55 mm long and, thanks to the sun-to-planet ratio $i = -0.5$, that the corresponding torque at the planet under the hypothesis of unitary efficiency is $0.728 \pm 0.14\,\mathrm{Nm}$.

Fig. 18 shows one of the functionality tests done with the ball screw spline gripper. The gripper started in the *grasping* mode where the linear motion generated by the screw caused the fingers to close to grasp the valve knob. At about 3 s, it is possible to observe the torque slowly rising in magnitude as soon as the fingers make contact with the knob. At 6.97 s the motor torque peaked after the knob was firmly grasped, triggering the bistable mechanism to the *twisting* mode. The gripper then kept loosening the valve knob until 18.00 s when the motor reached its target position and began returning to the starting angular position. As a result, the gripper began tightening the knob to close the valve. At 29.27 s, the torque required to close the valve peaked enough to trigger the transition to releasing the grasp on the knob. After that, the gripper fingers kept opening until the end of the test.

A mean maximum torque of $0.247 \pm 0.010\,\mathrm{Nm}$ was observed at the twisting to grasping mode transition while closing the valve. Instead, a mean minimum torque of $-0.194 \pm 0.011\,\mathrm{Nm}$ was recorded while transitioning between grasping and twisting during the valve opening phase. The significantly lower standard deviation in this prototype ($< 5\%$ of the mean) highlights the superior repeatability of the magnetic latching mechanism compared to the mechanical ball-detent version. In this case, estimating the grasping force

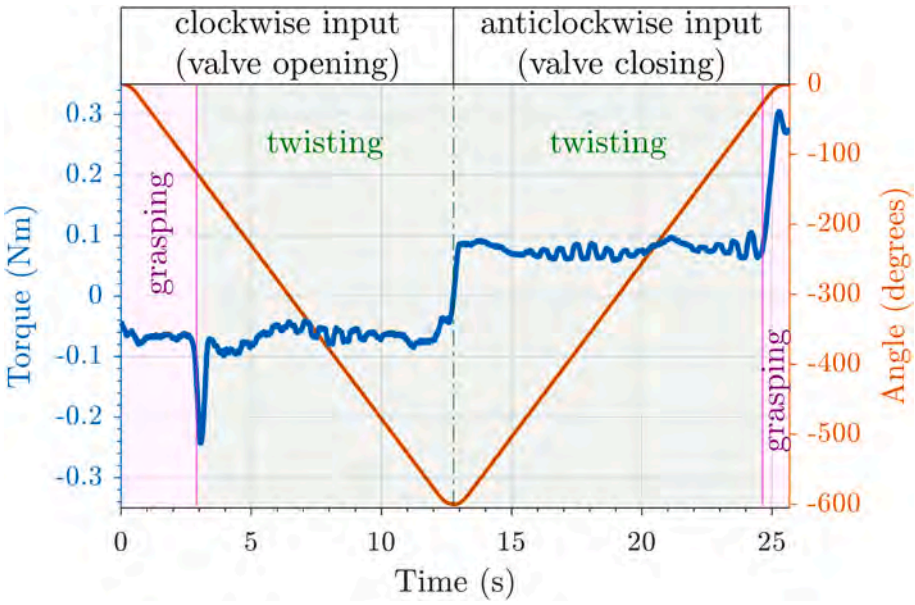

Fig. 17. Functionality test of the gripper based on the epicyclic gear transmission opening and closing a valve.

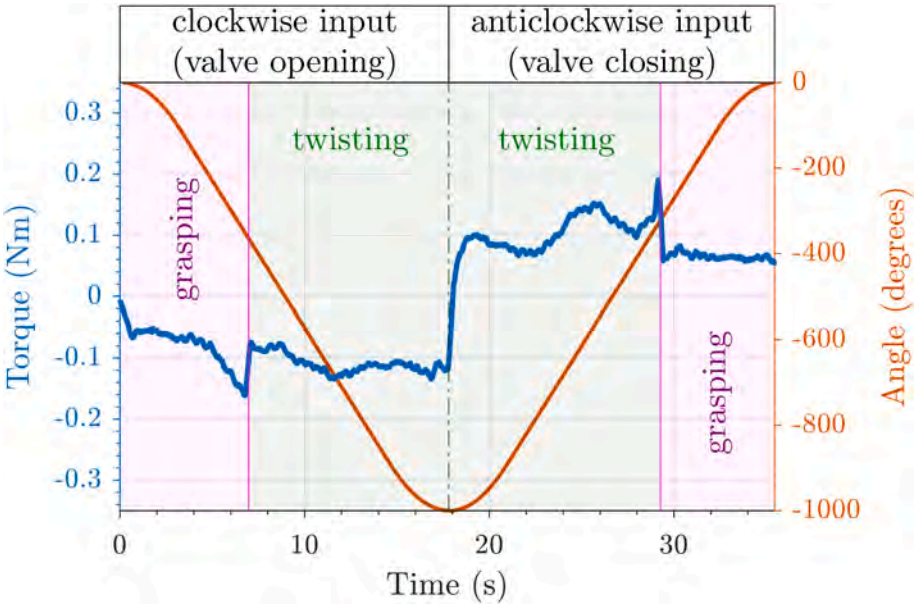

Fig. 18. Functionality test of the gripper based on the ball screw spline transmission, opening and closing a valve.

is not straightforward, as the finger mechanism of this prototype has its own transmission ratio, and it is not constant, but it changes as a function of the finger closure angle. However, assuming unitary transmission efficiency again and given $p = 5$ mm, the force applied to the finger mechanism and corresponding to the input torque is about 38.8 ± 0.22 N. Given the finger geometry and the valve size, and thus the instantaneous transmission ratio of the mechanism, the grasping force is about 29.76 ± 0.18 N. The fact that the gripping force is practically double that of the other mechanism also explains why there are no perceptible slippage effects with this design compared to the other one.

6. Discussion

Both prototypes successfully validated the concept of integrating an MRUM architecture, that is, a torque-driven bistable mechanism to automatically switch between two alternative output motions of a 2-DoF transmission. In particular, both prototypes were able to open and close a wine sample valve (i.e., a realistic representative use case scenario) using a single position-controlled input motion. This experimental success suggests that such grippers could be integrated on a robotic manipulator or even a mobile

manipulator to perform two different tasks with a single robotic gripper while automatically switching between them. This may be particularly beneficial to reduce weight and bulkiness at the end of the robotic manipulator.

When comparing the two solutions, the ball screw spline gripper, despite its more unique and complex mechanical transmission and the added complexity of magnetic interaction, proved to be the most repeatable, compact and lightweight prototype. In contrast, the epicyclic gear gripper resulted in a much more complex assembly, in particular due to the challenge of integrating a compact bistable mechanism within the limited volume of the planetary gear train.

While the prototypes successfully validated the MRUM concept, several physical and operational limitations were identified that provide a roadmap for future optimisation.

The epicyclic gear gripper was particularly affected by synchronisation issues between detents and recesses of the bistable subsystem during mode transition. The limited number of detents (originally 8, later increased to 24 with a ratchet) meant that the detents and recesses were not always perfectly aligned at the moment of transition, leading to occasional, but not task-critical, mechanical stuttering. Furthermore, this limited angular resolution resulted in discrete finger positions, which restricted the gripper's ability to properly keep the valve grasped, partially reducing the actual grasping force after triggering the mode switching. These positioning issues were compounded by a significant disparity in grasping force. Experimental data indicate that the ball screw spline gripper produces nearly double the grasping force of the epicyclic prototype. This explains why finger slippage relative to the knob was observed more frequently in the epicyclic design; the lower force was often insufficient to compensate for the suboptimal finger-to-object alignment caused by the detent resolution.

It is important to note that these issues are strictly related to the design parameter of the assembled prototype. They could be significantly mitigated by increasing the number of detents in the torque limiters. However, this means that the prototype should grow in its radial dimension to accommodate more detents of the same size. As an alternative, the bistable element could be redesigned to operate with smaller detents, allowing a higher number of detents within the same volume. In this respect, it is interesting to note that, given the bistable curved beam, higher torque thresholds require stiffer beams, and this generally allows for shorter beams, enabling more compact implementations.

On the contrary, the ball screw spline gripper proved to be much more robust to synchronisation-related issues, mostly because it was much easier to embed a larger number of magnets in a small volume and because the bistable mechanism does not only rely on contact, but the magnetic attraction and repulsion also have an effect at a distance. This characteristic largely explains why the ball screw spline gripper test results were much more repeatable than the ones with the epicyclic gear gripper.

The implementation of the ratchet clutch in the epicyclic prototype illustrates the utility of a task-driven approach for MRUM. While the ratchet is inherently unidirectional, it was a functionally valid solution for the valve-turning scenario because the specific sequence of mode transitions required by the task did not involve a torque overload in the ratchet's locked direction. This suggests that in practical applications, if the bistable latching mechanism can manage the specific mode transitions required by a given task, certain mechanical requirements, such as full bidirectionality, can be relaxed to achieve a simpler or more mechanically effective prototype.

In contrast, the fully bidirectional capabilities demonstrated by the ball-detent and magnetic coupling architectures represent a more universal class of MRUM. These solutions provide a foundation for grippers that are easily adaptable to diverse manipulation tasks where the direction of the reaction torque cannot be predicted or constrained. By choosing between task-specific hotfixes like the ratchet and universal solutions like the magnetic shuttle, designers can effectively balance the trade-offs between mechanical simplicity, resolution, and operational flexibility.

The variability observed in the experimental switching torques can be attributed to several interacting sources of uncertainty. First, the prototypes were primarily fabricated via PLA additive manufacturing, which introduces inherent print tolerances and surface roughness that affect the consistent frictional behaviour of the sliding components. Second, the limited angular resolution of the mechanical detents (the 'synchronisation issue' mentioned previously) means that the mechanism occasionally struggled to achieve proper meshing at the exact moment of transition, leading to momentary stuttering and variations in the required triggering torque. Third, the manual reset of the valve between trials introduced minor inconsistencies in the initial finger-to-knob orientation and contact conditions.

Notably, the performance of the ball screw spline prototype suggests that the magnetic latching mechanism is significantly more robust to these factors. Because the magnetic attraction and repulsion act over a distance rather than relying solely on discrete mechanical contact, the system is less sensitive to misalignment and surface wear, resulting in the high level of repeatability demonstrated in our results.

A critical consideration for the operational robustness of MRUM is its sensitivity to input dynamics. While the mode transitions are designed to be triggered by environmental resistance (reaction torque), high input accelerations can generate inertial torques that may prematurely trigger the bistable latch. Both grippers were tested at relatively low speeds and accelerations. However, it may be possible that a sufficiently large acceleration input may trigger the bistable subsystem. This is clearly an undesired behaviour; thus, the input motion acceleration should be properly controlled. At the same time, this particular behaviour could also be exploited to become an interesting feature: it could be possible to switch between modes on demand by intentionally accelerating over the threshold, leading to the switch between modes without relying only on the interaction of the gripper with the environment.

The inertial torque $T_{inertial}$ acting on the 2-DoF transmission–driven by the total moment of inertia J of the rotating components and their angular acceleration $\dot{\omega}$ is expressed as

$$T_{inertial} = J\dot{\omega} \tag{31}$$

To prevent unintended switching, the input motion must be constrained such that $T_{inertial}$ remains significantly below the threshold torque T_{thres}

$$T_{thres} > |T_{inertial}| = J|\dot{\omega}|, \tag{32}$$

which implies that the angular acceleration magnitude must be limited to:

$$|\dot{\omega}| < \dot{\omega}_{limit} = \frac{T_{thres}}{J}. \tag{33}$$

As mentioned before, this dynamic behaviour offers a unique opportunity for "on-demand" switching: by intentionally exceeding the acceleration limit, the actuator could trigger a mode change without requiring physical contact with an object, effectively embedding "mechanical intelligence" into the end-effector's control logic.

To assess the magnitude of the dynamic effects regarding switching due to only acceleration, consider the epicyclic gripper prototype presented in this study. Based on the CAD model, the moment of inertia seen by the motor in the twisting mode is approximately $J_{epi,twist} \approx 7.9 \times 10^{-4}\,\mathrm{kg \cdot m^2}$. Given the average measured threshold torque of $T_{thresh,twist} = 0.323\,\mathrm{Nm}$, (33) yields a triggering acceleration of $\dot{\omega}_{limit,twist} \approx 409\,\mathrm{rad/s^2}$. Similarly, in the grasping mode, the estimated moment of inertia is $J_{epi,grasp} \approx 1.6 \times 10^{-4}\,\mathrm{kg \cdot m^2}$, and with an average threshold torque of $T_{thresh,grasp} = 0.364\,\mathrm{Nm}$, the corresponding triggering acceleration is $\dot{\omega}_{limit,grasp} \approx 2275\,\mathrm{rad/s^2}$.

The maximum angular acceleration of the Dynamixel XH540-W150 servo-motor is limited by software at approximately $0.38\,\mathrm{rad/s^2}$, which is significantly lower than the values required to trigger an unintended switch. Consequently, this phenomenon could not be experimentally validated. More generally, the moments of inertia involved in these small, predominantly plastic prototypes are sufficiently low that the acceleration required to trigger the latching mechanism is particularly high. Furthermore, structural limitations inherent to 3D-printed (PLA) components precluded experimental validation at high accelerations, even with alternative actuators, to avoid potential damage to the prototypes.

To evaluate the practical advantages and limitations of the proposed MRUM architecture, it is useful to compare it against the baseline standard of a conventional fully-actuated end-effector (e.g., a 1-DoF gripper mounted on a 1-DoF wrist). The primary advantage of the MRUM approach is the reduction in hardware and control complexity. By utilising a single actuator for both grasping and continuous twisting, the system eliminates the weight, cost, and cabling requirements of a second motor and its associated drive electronics. Furthermore, the mode switching is governed by mechanical logic, specifically, the passive response to environmental torque, which removes the need for contact sensors, encoders, or high-level software logic to coordinate the transition between grasping and manipulation. However, these benefits involve specific trade-offs:

- Torque Capability: In a standard 2-actuator system, the maximum twisting torque is limited only by the wrist motor's capacity. In an MRUM, the twisting torque is bounded by the bistable threshold T_{thres}; exceeding this limit triggers a mode switch rather than continuing the rotation.
- Controllability: While the MRUM simplifies autonomous tasks like valve turning, it lacks the selective decoupling of a 2-actuator system. A standard wrist can rotate without grasping, whereas the MRUM is designed for tasks where these actions are sequential and task-dependent.
- Efficiency: The current proof-of-concept prototypes, being 3D-printed and non-optimised, likely exhibit lower transmission efficiency than professional-grade gearboxes. However, the proposed architecture offers a compact, single-actuator solution, which effectively maximises the utility of a single power source to drive multiple degrees of freedom.

This architectural comparison confirms that MRUM-based grippers are not intended to replace all general-purpose end-effectors but are highly effective alternatives for specialised mobile manipulation tasks where minimising weight and control overhead at the distal end of a robotic arm is a priority.

7. Conclusions

This paper presented a novel underactuated gripper architecture, named Mode-Retentive Underactuated Mechanisms (MRUM), capable of automatically switching between grasping and continuous bidirectional rotation using a single actuator. The proposed approach relies on a torque-driven bistable subsystem that selectively engages one output of a 2-DoF transmission while locking the other, enabling mode switching solely based on the reaction torque experienced during operation. Two alternative transmission solutions, a planetary gear train and a ball screw spline mechanism, were introduced, together with two corresponding implementations of the torque-driven latch, demonstrating the generality of the proposed concept.

Two physical prototypes were designed and fabricated to validate the working principle. Experimental results confirmed that both grippers could reliably transition between grasping and twisting modes and perform a representative task involving the opening and closing of a manual valve without any sensing or active control logic. While the two solutions exhibited different mechanical characteristics and practical trade-offs, both successfully demonstrated the feasibility of integrating a torque-driven bistable mechanism with a 2-DoF transmission to achieve autonomous mode selection.

Overall, the presented results validate the proposed mechanical concept and highlight its potential for applications requiring both secure grasping and controlled rotational manipulation with minimal actuation complexity. By embedding task-dependent decision-making directly into the mechanical design, this approach offers a compact and lightweight alternative to properly-actuated grippers, or even overly-actuated grippers, and provides a foundation for future developments of automatic task-adaptive mechanical end-effectors for robotic manipulation tasks.

CRediT authorship contribution statement

Andrea Botta: Writing – original draft, Visualization, Validation, Software, Methodology, Investigation, Formal analysis, Data curation, Conceptualization; **Luigi Tagliavini:** Writing – review & editing, Visualization, Validation, Methodology, Investigation, Formal analysis, Data curation, Conceptualization; **Francesco Amodio:** Writing – review & editing, Validation, Methodology, Investigation; **Daniel Pacheco Quinones:** Writing – review & editing, Validation, Formal analysis; **Danilo Stimolo:** Writing – review & editing, Validation, Methodology, Investigation, Formal analysis; **Giuseppe Quaglia:** Writing – review & editing, Supervision, Resources, Project administration, Formal analysis; **Daniela Maffiodo:** Writing – review & editing, Supervision, Resources, Project administration, Funding acquisition, Formal analysis, Conceptualization.

Declaration of competing interest

The authors declare that they have no known competing financial interests or personal relationships that could have appeared to influence the work reported in this paper.

Acknowledgment

This publication is part of the project NODES, which has received funding from the MUR - M4C2 1.5 of PNRR with grant agreement no. ECS00000036.

Data availability

Data will be made available on request.

Supplementary material

Supplementary material associated with this article can be found in the online version at 10.1016/j.mechmachtheory.2026.106530.

References

[1] J. Li, T. Liao, H. Nigatu, H. Guo, G. Lu, H. Dong, Under-actuated robotic gripper with multiple grasping modes inspired by human finger, in: 2024 IEEE/RSJ International Conference on Intelligent Robots and Systems (IROS), IEEE, 2024, pp. 5297–5302. ISSN: 2153-0866, https://ieeexplore.ieee.org/abstract/document/10802532/media. https://doi.org/10.1109/IROS58592.2024.10802532

[2] J. Choi, J. Won, W. Lee, T. Seo, An underactuated gripper design and evaluation with linkage-based system for a front approach, Robot. Auton. Syst. 191 (2025) 105005. https://doi.org/10.1016/j.robot.2025.105005

[3] G.-S. Kim, H.S. Kim, SA gripper: an underactuated gripper with a 6-bar mechanism in a parallelogram structure, Proc. Inst. Mech. Eng. C: J. Mech. Eng. Sci. (2025) 09544062251350557. Publisher: IMECHE, https://doi.org/10.1177/09544062251350557

[4] T. Laliberté, C.M. Gosselin, Simulation and design of underactuated mechanical hands, Mech. Mach. Theory 33 (1) (1998) 39–57. https://doi.org/10.1016/S0094-114X(97)00020-7

[5] I. Hussain, F. Renda, Z. Iqbal, M. Malvezzi, G. Salvietti, L. Seneviratne, D. Gan, D. Prattichizzo, Modeling and prototyping of an underactuated gripper exploiting joint compliance and modularity, IEEE Robot. Autom. Lett. 3 (4) (2018) 2854–2861. https://doi.org/10.1109/LRA.2018.2845906

[6] N. Mouazé, L. Birglen, Bistable compliant underactuated gripper for the gentle grasp of soft objects, Mech. Mach. Theory 170 (2022) 104676. https://doi.org/10.1016/j.mechmachtheory.2021.104676

[7] X. Sun, S. Yang, Y. Li, W. Chen, Y. Jin, A low-cost underactuated compliant gripper with multifunctional jaws for precision manipulation, Sens. Actuat. A: Phys. 366 (2024) 115047. https://doi.org/10.1016/j.sna.2024.115047

[8] A. Kakogawa, H. Nishimura, S. Ma, Underactuated modular finger with pull-in mechanism for a robotic gripper, in: 2016 IEEE International Conference on Robotics and Biomimetics (ROBIO), 2016, pp. 556–561. https://doi.org/10.1109/ROBIO.2016.7866381

[9] T. Ko, A tendon-driven robot gripper with passively switchable underactuated surface and its physics simulation based parameter optimization, IEEE Robot. Autom. Lett. 5 (4) (2020) 5002–5009. https://doi.org/10.1109/LRA.2020.3005131

[10] G. Quaglia, L. Tagliavini, G. Colucci, A. Vorfi, A. Botta, L. Baglieri, Design and prototyping of an interchangeable and underactuated tool for automatic harvesting, Robotics 11 (6) (2022) 145. Number: 6 Publisher: Multidisciplinary Digital Publishing Institute. https://doi.org/10.3390/robotics11060145

[11] T. Nishimura, Y. Suzuki, T. Tsuji, T. Watanabe, 1-degree-of-freedom robotic gripper with infinite self-twist function, IEEE Robot. Autom. Lett. 7 (3) (2022) 8447–8454. https://doi.org/10.1109/LRA.2022.3187823

[12] T. Nishimura, K. Ueno, T. Watanabe, Motor-less robotic gripper: driving mechanism by robotic manipulator movement, IEEE Access 13 (2025) 23913–23923. https://doi.org/10.1109/ACCESS.2025.3538001

[13] J. Jang, J. Park, J.-K. Lee, J.-H. Ryu, SPINE Gripper: A Twisted Underactuated Mechanism-based Passive Mode-Transition Gripper, 2026. arXiv:2601.06833 [cs.RO].

[14] J.-H. Meng, I. Yoon, S.-J. Park, J.-B. Song, A gripper capable of screw fastening and gripping with a single driving source, Int. J. Control Autom. Syst. 22 (9) (2024) 2882–2890. https://doi.org/10.1007/s12555-023-0859-8

[15] A. Seino, F. Tokuda, A. Kobayashi, K. Kosuge, Passive actuator-less gripper for pick-and-place of a piece of fabric, IEEE/ASME Trans. Mechatron. 30 (6) (2025) 5856–5866. https://doi.org/10.1109/TMECH.2025.3543557

[16] J. Qiu, J.H. Lang, A.H. Slocum, A curved-beam bistable mechanism, J. Microelectromech. Syst. 13 (2) (2004) 137–146. https://doi.org/10.1109/JMEMS.2004.825308

[17] H. Hussein, P. Le Moal, G. Bourbon, Y. Haddab, P. Lutz, Modeling and stress analysis of a pre-shaped curved beam: influence of high modes of buckling, Int. J. Appl. Mech. 7 (04) (2015) 1550055. https://doi.org/10.1142/S1758825115500556

[18] H. Hussein, P. Le Moal, R. Younes, G. Bourbon, Y. Haddab, P. Lutz, On the design of a preshaped curved beam bistable mechanism, Mech. Mach. Theory 131 (2019) 204–217. https://doi.org/10.1016/j.mechmachtheory.2018.09.024

[19] T. Lubin, S. Mezani, A. Rezzoug, Simple analytical expressions for the force and torque of axial magnetic couplings, IEEE Trans. Energy Convers. 27 (2) (2012) 536–546. https://doi.org/10.1109/TEC.2012.2183372